Gravity-Driven flow of evaporating thin liquid films over substrates with topography

Gaskell, P.H.*, Jimack, P.K.**, Sellier, M.* and Thompson, H.M.*

*Engineering Fluid Mechanics Research Group, School of Mechanical Engineering, University of Leeds, Leeds, UK.
**School of Computing, University of Leeds, Leeds, UK.

Abstract

This paper considers gravity-driven flow of thin liquid films over substrates with topography, the non-evaporating case of which has recently been studied experimentally (Decre and Baret 2003) and numerically (Gaskell et al 2003a), and extends the latter to consider the effects of solvent evaporation. In contrast to most previous studies, which have used semi-implicit time-splitting methods to solve the governing nonlinear time-dependent lubrication equations, the present one uses an efficient Multigrid method with adaptive time-stepping. Numerical solutions illustrating the effects of solvent evaporation, and the associated increase in viscosity, for the chosen test problem are presented here for the first time.

1. Introduction

The fluid dynamical behaviour of thin liquid films, whether forced to spread over a solid surface or deposited as a distinct pattern, is of enormous significance in many manufacturing processes. Much is now known about the deposition of films on flat, homogeneous substrates and several recent studies have been directed towards the flow of films forced (gravitationally or centrifugally) to flow over surfaces containing topographical features, which may either be regular and desired (patterned) or unwanted (a random scratch or a speck of dust). Such flows arise, for example, in the electronics sector during the manufacture of micro-devices, sensors, printed circuits, displays etc., when successive deposition of several thin layers may lead to non-uniform coating thickness.

The present paper considers the particular case of gravity-driven flow of thin liquid films over well defined topography, as indicated in Figure 1, in which

a thin layer of liquid, thickness h(x,y), flows over a topography s(x,y) on a substrate inclined at an angle α to the horizontal. It builds on and extends the experimental study by (Decre and Baret 2003) into the flow

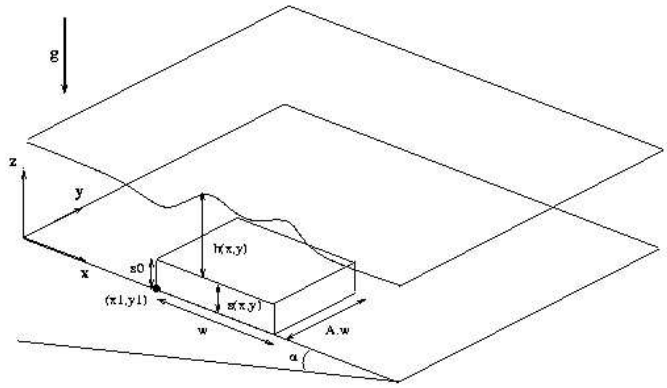

Figure 1: Gravity-driven flow down an inclined plane with topography

of thin water films over inclined substrates and extends the recent numerical analysis of these flows, by (Gaskell et al 2003b), to consider the effects of solvent evaporation. The motivation for this study is that in several industrial processes the applied liquid is composed of a resin (the functional material) dissolved in a volatile solvent from which the drying process of solvent evaporation leads to significant increases in the viscosity of the liquid, leaving ultimately a solid resin film on the substrate.

The effects of solvent evaporation on the dynamics of thin film flows have been considered by several previous authors in a variety of physical contexts. Overdiep (1986), for example, showed that evaporation can cause the free surface of some solvent-based alkyd paints to undergo reversal in which initial peaks in the free surface become troughs and vice-versa. Meyerhofer (1978) is credited as being the first to model the effects of solvent evaporation and variable viscosity on the thickness of dried films during spin coating and showed that the thinning of films occurs in two stages. The first is convection dominated while the second, later stage is dominated by evaporation. This analysis was subsequently extended to consider the effects of concentration gradients across the film (Bornside et al 1989) and topography (Stillwagon and Larson 1990). More recent studies have considered evaporative effects on the flow of thin paint layers (Howison et al

1997), and the stability and dynamics of evaporating thin films on partially and completely wetting horizontal substrates (Schwartz et al 2001).

2. Mathematical Model

Scaling film thicknesses by that for the fully-developed flow down an inclined plane, $H_0 = (3\mu Q / \rho g \sin\alpha)^{1/3}$, lengths by the Capillary length $L_0 = (\sigma H_0 / 3\rho g \sin\alpha)^{1/3}$, velocities by the surface velocity of the fully-developed flow $U_0 = \rho g \sin\alpha H_0^2 / 2\mu$, and the evaporation rate by εU_0 (where $\varepsilon = H_0 / \beta L_0$ and βL_0 is the extent of the substrate with β=50) enables the time evolution of the film thickness h and pressure p to be given respectively by (Gaskell et al 2003b)

$$\frac{\partial h}{\partial t} = \frac{\partial}{\partial x}\left[\frac{h^3}{3\tilde{\mu}}\left(\frac{\partial p}{\partial x} - 2\right)\right] + \frac{\partial}{\partial y}\left[\frac{h^3}{3\tilde{\mu}}\left(\frac{\partial p}{\partial y}\right)\right] - e \qquad (1)$$

$$p = -6\nabla^2 (h + s) + 2\sqrt[3]{6Ca}\cot\alpha \qquad (2)$$

where $\tilde{\mu} = \mu / \mu_0$ is the dimensionless viscosity ratio with respect to the initial viscosity μ_0, e is the dimensionless (constant) evaporation rate, s is the dimensionless topography profile and $Ca = \mu_0 U_0 / \sigma$. Following Howison et al (1997), the equation for the mass of solvent yields

$$\frac{\partial c_s}{\partial t} = \frac{\partial}{\partial x}\left[\frac{h^3}{3\tilde{\mu}}\left(\frac{\partial p}{\partial x} - 2\right)\right]\frac{\partial c_s}{\partial x} + \frac{\partial}{\partial y}\left[\frac{h^3}{3\tilde{\mu}}\left(\frac{\partial p}{\partial y}\right)\right]\frac{\partial c_s}{\partial y} - \frac{e(c_s - 1)}{h} \qquad (3)$$

where c_s is the solvent concentration. In the solutions discussed later the base fluid properties are those of water, namely $\mu_0 = 0.001$ Pas, ρ =1000kg/m^3 and σ =0.07N/m is assumed constant so that Marangoni effects are neglected. The viscosity dependence on solvent concentration is given by the exponential law $\mu(c_s) = \mu_0 e^{a(c_0 - c_s)}$ (Schwartz et al 2001) where a=70 and the initial solvent concentration c_0 =0.7.

3. Numerical Method

3.1 Discretised Form of the Governing Equations

The governing equations (1)-(3) are discretised spatially using second order accurate Finite Differences on a square computational domain with $0 \leq (x,y) \leq 1$, which yields

$$\frac{\partial h_{i,j}}{\partial t} = \frac{1}{\Delta^2}\left[\frac{h^3}{3\tilde{\mu}}\Big|_{i+1/2,j}(p_{i+1,j} - p_{i,j}) - \frac{h^3}{3\tilde{\mu}}\Big|_{i-1/2,j}(p_{i,j} - p_{i-1,j}) + \right.$$

$$\left.\frac{h^3}{3\tilde{\mu}}\Big|_{i,j+1/2}(p_{i,j+1} - p_{i,j}) - \frac{h^3}{3\tilde{\mu}}\Big|_{i,j-1/2}(p_{i,j} - p_{i,j-1})\right]$$

$$+ 2\,h^2{}_{i,j}\left(\frac{h_{i+1,j} - h_{i-1,j}}{2\Delta}\right) - e \qquad (4)$$

$$p_{i,j} + \frac{6}{\Delta^2}\Big[(h_{i+1,j} + s_{i+1,j}) + (h_{i-1,j} + s_{i-1,j}) + (h_{i,j+1} + s_{i,j+1}) +$$

$$(h_{i,j-1} + s_{i,j-1}) - 4(h_{i,j} + s_{i,j})\ \Big] - 2\sqrt[3]{6}\,N\,(h_{i,j} + s_{i,j}) = 0 \qquad (5)$$

$$\frac{\partial c_{si,j}}{\partial t} = \frac{h^3{}_{i,j}}{12\tilde{\mu}_{i,j}\,\Delta^2}\Big[(p_{i+1,j} - p_{i-1,j})(c_{si+1,j} - c_{si-1,j}) +$$

$$(p_{i,j+1} - p_{i,j-1})(c_{si,j+1} - c_{si,j-1})\Big] - 2\frac{h_{i,j}{}^2}{6\tilde{\mu}_{i,j}\Delta}(c_{si+1,j} - c_{si-1,j})$$

$$+ e\frac{(c_{si,j} - 1)}{h_{i,j}} \qquad (6)$$

where the $\frac{h^3}{3\tilde{\mu}}\Big|_{i\pm1/2,j} = \frac{1}{2}\left(\frac{h^3}{3\tilde{\mu}}\Big|_{i\pm1,j} + \frac{h^3}{3\tilde{\mu}}\Big|_{i,j}\right)$ terms are referred to as the pre-factors of the interpolation.

3.2 Temporal Discretisation

Ideally, time-stepping schemes for the numerical solution of transient flows should be both *efficient* and *accurate*. The former ensures that small time steps are avoided when the solution varies slowly while the latter should enable the error to be controlled throughout the solution process. Most

previous studies of lubrication flows have used time-splitting algorithms employing alternate sweeps in each direction to enable far larger time steps to be used than would be the case with simple, explicit schemes (Schwartz et al 2001.

Few studies have ever attempted to control the accuracy of time-stepping schemes for the lubrication equations. This study uses efficient time-stepping based on local error estimates from an implicit, second-order method that reduces to Heun's method in the case of a fixed time step. The reader is referred to Gaskell et al (2003a) for further details on this method.

3.3 The Multigrid Method

Multigrid methods are fast solvers, the essence of which is to use simple iterative techniques as a smoother, not as a solver, to reduce high frequency errors on the computational grid while lower frequency errors are smoothed out on a succession of coarser computational grids. Briefly, a hierarchy of grids is defined, $G^0, G^1, ..., G^L$ say where the grid spacing halves from one grid to the next and where G^0 denotes the coarsest grid and G^L the finest. At each time step the errors whose wavelengths are less than or equal to the grid spacing of grid G^i are reduced by applying a fixed number of V cycles of the iterative technique so that at the end of the Multigrid process the remaining errors are small.

The nonlinear discrestised Eqs (4)-(6) are solved using a combination of the Full Approximation Storage (FAS) and the Full Multigrid Technique. This method is preferred over the usual time-stepping approach since if offers both improved efficiency (CPU time for a typical time step is proportional to the number of unknowns, N) and stability, the latter allowing larger time steps to be used. The coarsest grid level G^0 used is a 17x17 one and Multigrid solutions are reported where the finest grid has 257x257 nodes in each direction. Further details of the Multigrid technique can be found in Gaskell et al (2003a).

4. Results

Examples of two- and three-dimensional flows are given which extend the previous numerical analysis (Gaskell et al 2003b) to cases with solvent evaporation. Figure 2 shows an example of a flow over a step-up topography of height $50\mu\text{m}$ when $H_0 = 100\mu\text{m}$ and $e = 0.05$. It shows how the film thickens compared with the non-evaporating case, due to a viscosity rise (shown by the dashed line) across the film.

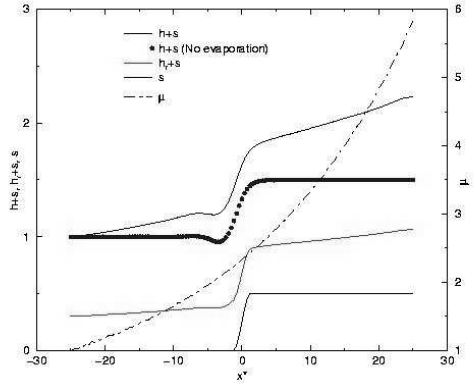

Figure 2: Two-dimensional flow over a step-up topography with evaporation.

The final two figures show how the three-dimensional flow over a square trench topography of depth 100μm with $H_0 = 100\mu$m and 7.8mm sides is affected by solvent evaporation. Figure 3 compares the free surface profile along the streamwise topography centerline for $e = 0.05$ with the non-evaporative case. Once again, the viscosity rise in the downstream direction (shown by the dashed line) leads to a corresponding rise in the free surface profile and in the resin profile, h_r+s.

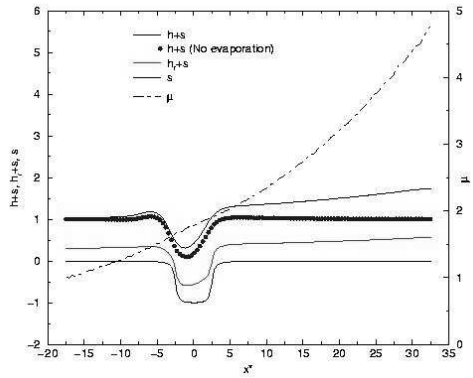

Figure 3: Free surface profiles along the streamwise topography centreline

Figure 4 shows spanwise free surface and viscosity profiles at two different downstream locations as a function of the evaporation rate with $0 \le e \le 0.1$.

Figures 4(a) and 4(b) show the free surface profiles at the edge of the topography and at 3.9mm further downstream from the edge of the topography respectively. As expected, they reveal that the free surface rises progressively as evaporation rate increases and that the effects of the topography on the free surface have almost disappeared further downstream. Figures 4(c) and 4(d) consider the corresponding variation in viscosity. Interestingly, they show that the peaks in viscosity generated at the edges of the topography are preserved further downstream.

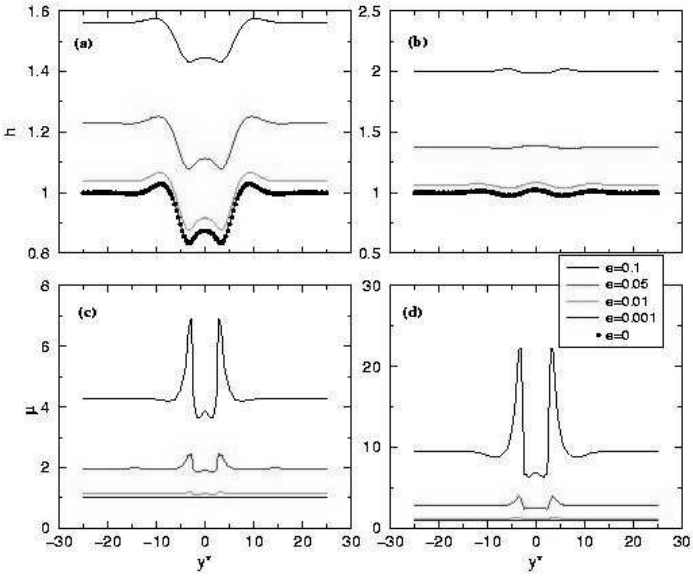

Figure 4: Spanwise free surface and viscosity profiles at the downstream edge of the topography ((a) and (c)) and a further 3.9mm downstream ((b) and (d))

5. Conclusions

A wide range of gravity-driven flows of thin liquid films over substrates with topography are modelled accurately using the nonlinear lubrication equations which can now be solved efficiently via a Multigrid method with adaptive time-stepping. The Multigrid solver has been fully validated against experimental data for the non-evaporative case and the present study presents the first analysis of the industrially-important case with solvent evaporation.

Solutions are presented which show that the viscosity rise associated with solvent evaporation leads to a thickening of the film and that the initial free surface disturbances caused by a topography are dissipated further downstream but that the viscosity peaks caused by the topography are preserved. There is now a need to obtain accurate experimental data for the evaporative case with which to compare the numerical predictions and to assess the importance of Marangoni effects which have been neglected here.

6. References

Decre, M and Baret, J-C., 2003, Gravity-driven flows of low viscosity liquids over two-dimensional topographies. *J. Fluid Mech*., **487**, p 147

Gaskell, P.H., Jimack, P.K., Sellier, M. and Thompson. H.M, 2003a. Efficient and accurate time adaptive multigrid simulations of droplet spreading. *Int. J. Num. Meth. Fluids- in press.*

Gaskell, P.H., Jimack, P.K., Sellier, M., Thompson, H.M., M.C.T. Wilson, 2003b. Gravity-driven flow of continuous thin liquid films on non-porous substrates with topography. *Journal of Fluid Mechanics – in press.*.

Overdiep, W.S., 1986, The levelling of paints. *Prog. Org. Coat.*, **14**, p 159

Meyerhofer D., 1978, Characteristics of resist films produced by spinning. *J. Appl. Phys.*, **49**, p 3993.

Bornside, D.E., Macosko, C.W. and Scriven, L.E., 1989, Spin coating – one-dimensional model. *J. Appl. Phys.*, **66**, p 5185.

Stillwagon. L.E., Larson, R.G., 1988, Fundamentals of topographic surface levelling. *J. Appl. Phys*., **63**, p 5251.

Howison, S.D., Moriarty, J.A., Ockendon, J.R. and Terril, E.L., 1997, A mathematical model for drying paint layers. *J. Eng. Math.*, **32(4)**, p 377.

Schwartz, L.W., Valery Roy, R., Eley, R.R. and Petrash, S. 2001, Dewetting patterns in a drying liquid film, *Journal of Colloid and Interface Science*, **234**, 363-374.